

Cite this article as: Yin Yuhuan, Wang Yipeng, Gao Han, et al. Stimulated Pulse Keyhole Behavior in Double-Pulsed VPTIG Welding of AA2219 High Strength Aluminum Alloy[J]. Rare Metal Materials and Engineering, 2022, 51(10): 3596-3601.

ARTICLE

# Stimulated Pulse Keyhole Behavior in Double-Pulsed VPTIG Welding of AA2219 High Strength Aluminum Alloy

Yin Yuhuan<sup>1</sup>, Wang Yipeng<sup>2</sup>, Gao Han<sup>1</sup>, Zhong Hao<sup>3</sup>, Qi Bojin<sup>3</sup>, Zhang Tiemin<sup>4</sup>, Cong Baoqiang<sup>3</sup>

<sup>1</sup> Shanghai Aerospace Equipments Manufacturer Co., Ltd, Shanghai 200245, China; <sup>2</sup> Institute of Light Alloy and Processing, Faculty of Materials and Manufacturing, Beijing University of Technology, Beijing 100124, China; <sup>3</sup> School of Mechanical Engineering and Automation, Beihang University, Beijing 100191, China; <sup>4</sup> Beijing Spacecrafts, Beijing 100086, China

**Abstract:** Keyhole tungsten inert gas (K-TIG) welding is a variant of TIG welding, which can largely improve the weld penetration depth by forming keyholes inside the molten pool during welding. However, K-TIG welding is generally considered unsuitable for aluminum alloys due to their high thermal conductivity. A novel double-pulsed variable polarity TIG (DP-VPTIG) welding process was employed and the stable full penetration keyhole welding of 7 mm-thick AA2219 aluminum alloy was achieved. Keyhole dynamic evolution for DP-VPTIG was investigated based on visual sensing technology. Results indicate that in low-pulsed peak stage of DP-VPTIG process, the keyhole forms under the dominant role of the downward arc pressure against the upward surface tension and hydrostatic pressure acting on the surface of the molten pool, while the keyhole is closed as the upward surface tension and hydrostatic pressure become the dominant role in low-pulsed base stage. The periodic variation of low-frequency pulse in DP-VPTIG process stimulates a periodic keyhole behavior of “opening” and “closing” in the molten pool. The formation of keyhole is beneficial to the increase of weld penetration depth as the arc moves downwards along the keyhole and directly heats the solid metal under the molten pool. The keyhole size decreases with the increase of low-pulsed frequency.

**Key words:** keyhole welding; double pulses; gas tungsten arc welding; aluminum alloy

Aluminum alloys are widely used in aerospace, automobile and shipbuilding industries due to their excellent fracture toughness, high specific strength, good corrosion resistance and processing properties<sup>[1-3]</sup>. Welding processing is one of the most important manufacturing methods for the production of aluminium alloys, among which variable polarity tungsten inert gas welding (VPTIG) is extensively adopted owing to its cathode cleaning effect and stable welding process<sup>[4,5]</sup>. However, the weld penetration depth of TIG welding is shallow, and the arc energy density as well as the welding efficiency are relatively low attributed to its free-diverging arc<sup>[6]</sup>. The ways to enhance the welding efficiency of TIG mainly include the use of mixed shielding gases, the variation of conventional TIG process and the application of new processes<sup>[7]</sup>. Keyhole mode TIG, referred as K-TIG, is considered as an effective way to increase the penetration

depth<sup>[8]</sup>. The keyhole during K-TIG welding process is mainly formed by a high current value, normally exceeding 300 A, which is high enough for the arc pressure to penetrate through the liquid molten pool<sup>[9]</sup>. This process is particularly applied in the joining of mid-thick plates, generally in the range from 6 mm to 12 mm, without edge preparation and additional filler materials<sup>[10]</sup>. Therefore, the welding efficiency can be largely improved compared with conventional TIG welding process.

K-TIG welding has been successfully applied in the joining of Ti-6Al-4V titanium alloys and commercially pure titanium with thickness up to 13 mm by Lathabai et al<sup>[11]</sup>, 6.35 mm commercially pure zirconium by Lathabai et al<sup>[10]</sup>, mild steels in the range from 6 mm to 12 mm by Lohse et al<sup>[12]</sup>, 6.35 mm carbon steels by Olivares et al<sup>[13]</sup>, 10 mm AISI 316L stainless steels by Feng et al<sup>[14]</sup>, 5.5 mm C-Mn steel by Liu et al<sup>[15]</sup>, and 10.8 mm S32101 duplex stainless steels by Cui et al<sup>[16]</sup>.

Received date: October 28, 2021

Foundation item: National Natural Science Foundation of China (52075022); Shanghai Natural Science Foundation (19ZR1423300)

Corresponding author: Wang Yipeng, Ph. D., Assistant Professor, Institute of Light Alloy and Processing, Faculty of Materials and Manufacturing, Beijing University of Technology, Beijing 100124, P. R. China, E-mail: wyp092@163.com

Copyright © 2022, Northwest Institute for Nonferrous Metal Research. Published by Science Press. All rights reserved.

However, the materials available for K-TIG welding are mainly low thermal conductivity metals. There are almost no literatures reporting about the K-TIG for aluminium alloys. As Lathabai et al<sup>[10]</sup> stated, the critical factors for K-TIG are surface tension and thermal conductivity. As to aluminum alloys, the surface tension is quite low and the thermal conductivity is relatively high. When the heat input is increased through simply increasing the arc current, the volume of the weld pool will be greatly enlarged due to the high thermal conductivity, so it is difficult to stabilize the weld pool with a low surface tension when keyhole is formed inside the molten pool.

To improve the stability of K-TIG welding process, a large amount of research works have been carried out. Backing jet flow argon gas was employed in the keyhole welding of C-Mn steel<sup>[15]</sup>. Experimental results show that this process is beneficial to enhancing the stability of K-TIG welding process. High frequency current (38.6 kHz) was introduced in the K-TIG welding of Q345 steel<sup>[17]</sup>. It is proved that the current window is significantly expanded and the threshold current is largely reduced, compared with those of the constant current keyhole welding process. The low frequency pulsed current (1~1.5 Hz) is proved to be useful to effectively stabilize the keyhole welding of 304 stainless steel with a wider current window<sup>[18]</sup>. In general, the current waveform modulation is an effective way to stabilize the K-TIG welding process<sup>[19]</sup>. In this study, in order to realize the stable keyhole welding of aluminum alloys, the high-frequency current (20~80 kHz) and low-frequency current (0.5~5 Hz) were simultaneously modulated into the conventional variable polarity current, referred as DP-VPTIG. The evolution process of keyhole dynamic behavior in 7 mm AA2219 aluminum alloy was investigated by a CCD-based visual sensing system. The results provide a solid foundation for the application of K-TIG welding process in aluminum alloys.

## 1 Experiment

The experimental platform of the welding system is displayed in Fig. 1. This system mainly consists of a self-developed DP-VPTIG welding power supply, a screw motion mechanism, a welding robot, a welding torch and its water cooling system, shielding gas and real-time image acquisition system. The acquisition system was primarily composed of a CCD-based area-array camera (BASLER avA1000-120 km) with the sampling rate up to 120 frames per second, a data acquisition card and a computer controlling system. The CCD camera was equipped with an adjustable focal length industrial lens (Computer M5018-MP2). In order to filter out the interference caused by the strong arc light, a narrow-band interference filter with a central wavelength of 1064 nm and a bandwidth of 25 nm was installed on the lens. The camera was fixed behind the welding torch in the welding direction and maintained a certain downward tilt angle. It focused on the surface of the work-piece directly below the electrode. During the welding process, the welding torch remained stationary while the work-piece moved with the screw motion mechanism.

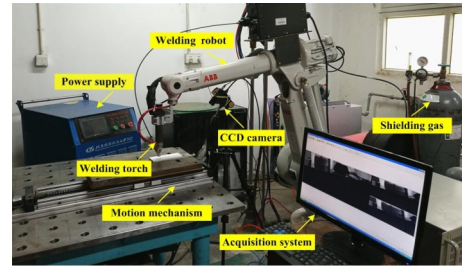


Fig.1 Experimental platform of the welding system

The schematic diagram of the current waveform of DP-VPTIG is shown in Fig.2. The conventional variable polarity current was modulated into 0.5~5 Hz ranged low-frequency pulse and high-frequency pulse, in the range of 20 kHz to 80 kHz, superposing in the positive stage.  $T_H$  is the period of variable polarity current,  $T_L$  is the period of low-frequency current,  $t_{Hn}$  is the duration of negative stage,  $t_{Hp}$  is the duration of positive stage,  $t_b$  is the duration of low-frequency pulse base stage,  $t_p$  is the duration of low-frequency pulse peak stage,  $I_{bn}$  is the negative current during  $t_b$ ,  $I_{bp}$  is the positive current during  $t_b$ ,  $I_{pn}$  is the negative current during  $t_p$ ,  $I_{pp}$  is the positive current during  $t_p$ .

The base metal employed was AA2219 aluminium alloy plate. The work-piece was machined into the dimension of 150 mm×60 mm×7 mm (length×width×thickness). The shielding gas was 99.99% pure argon, and the electrode adopted was cerium tungsten, with 4 mm in diameter and a 30 degree cone angle in the front tip. Since the effect of high-frequency pulsed current on arc behaviour and fluid flow of weld pool have been investigated, it has been proved that the high-frequency pulse can largely constrict the welding arc<sup>[20,21]</sup>, and effectively enhance the weld penetration<sup>[22,23]</sup>. Therefore, the parameters of high-frequency pulse were set as constant values with the purpose of improving the arc penetrating ability at a relatively low heat input. This study mainly focused on the effect of low-frequency pulse on the keyhole dynamic evolution process. The parameters used were: high-pulsed frequency of 20 kHz, duty cycle of 50%, amplitude of 80 A;  $T_H=100$  Hz,  $t_{Hp}:t_{Hn}=8:2$ ;  $T_L=0.5$  Hz,  $t_p:t_b=50\%$ ,  $I_{pp}/I_{pn}=360$  A,  $I_{bp}/I_{bn}=120$  A; shielding gas flow rate of 15 L·min<sup>-1</sup>, welding speed of 170 mm·min<sup>-1</sup>, the electrode tip to work-piece distance of 3 mm. The parameters selected above have been experimentally proven to successfully achieve a stable fully penetrated keyhole welding process.

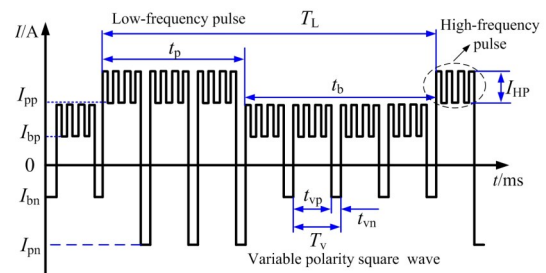


Fig.2 Schematic illustration of DP-VPTIG current waveform

Fig. 3 shows the image of weld pool and keyhole entrance captured by the camera. The sampling rate was 60 frames per second, and the resolution was  $340 \times 340$ . In order to quantitatively analyze the dynamic evolution of the keyhole behaviour, the weld pool width  $D_w$  and keyhole entrance size  $D_k$  were defined as feature sizes of weld pool and keyhole, respectively. A steel ruler was used as the reference size to determine the actual sizes of  $D_w$  and  $D_k$ . To avoid the measuring errors and ensure the repeatability, three images taken from different periods were used for the calculation of average value.

## 2 Results and Discussion

### 2.1 Keyhole dynamic evolution process

Fig. 4 shows the images captured in the low-pulsed peak stage  $t_p$  and corresponding weld pool width ( $D_w$ ) and keyhole size ( $D_k$ ). It can be seen that both the weld pool width and keyhole size exhibit a trend of increasing first and then gradually becoming stable in the duration of  $t_p$ . As the heat input is high in  $t_p$  due to the high current value, the weld pool width  $D_w$  monotonically increases from 8.6 mm at the beginning of  $t_p$  (100 ms) to 13.4 mm at the end of  $t_p$  (1000 ms). At the time of 100 ms, there is almost no obvious depression on the weld pool surface, meaning that keyhole does not form at the beginning of  $t_p$ . The weld pool surface is then depressed downwards along the thickness, accompanied with the liquid molten metal pushed to the rear and edge of the weld pool. Simultaneously, a keyhole forms in the center

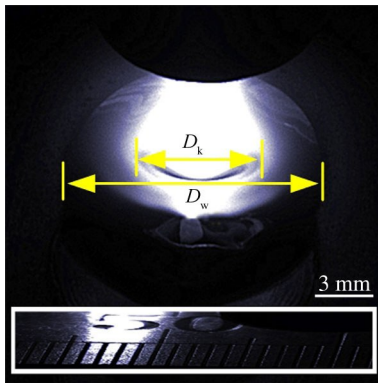


Fig.3 Measurement of weld pool width and keyhole size

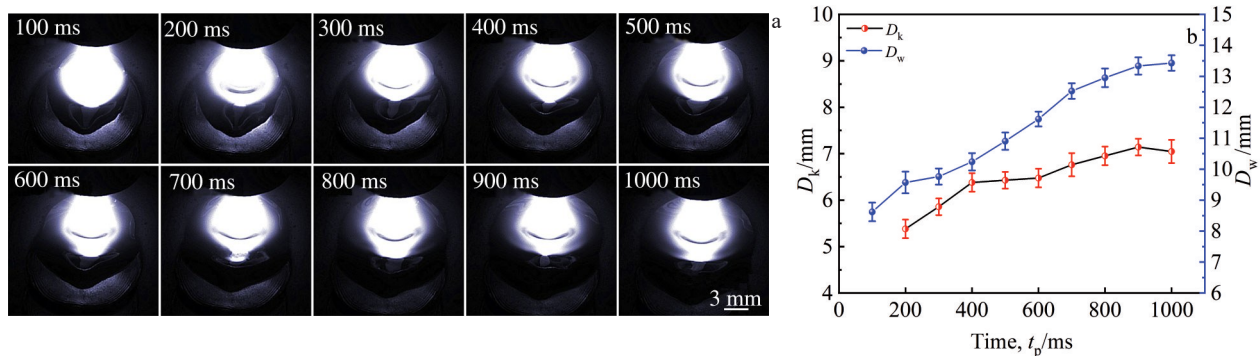


Fig.4 Keyhole appearance evolution process in low-pulsed peak stage  $t_p$  (a); weld pool width  $D_w$  and keyhole size  $D_k$  (b)

of the weld pool, just below the welding arc. The keyhole size  $D_k$  continuously increases from 5.4 mm to 6.8 mm with increasing pulse peak time from 200 ms to 400 ms. Then, the keyhole size gradually becomes stable at around 7 mm.

The images and corresponding weld pool width ( $D_w$ ) and keyhole size ( $D_k$ ) in low-pulsed base stage  $t_b$  are illustrated in Fig. 5. As the welding current switches from pulse peak to pulse base stage, the arc energy is significantly reduced owing to the dramatic reduction in the current value. The arc optical radiation is thus greatly weakened as revealed in the images. Consequently, the heat input to the base metal is drastically decreased, causing the molten pool to cool down and solidify from the rear and edge to the centre. Correspondingly, the weld width  $D_w$  decreases continuously from 11.2 mm at the beginning of  $t_b$  (1100 ms) to 6.9 mm at the end of  $t_b$  (2000 ms). Meanwhile, the depression of the weld pool surface decreases as the welding arc moves upwards along the thickness. The liquid molten metal flows back from the rear and edges of the weld pool, and fills the keyhole. From 1300 ms, the keyhole is completely closed ( $D_k=0$ ).

The forces acting on the surface of the weld pool is the key factor in the evolution of keyhole<sup>[19]</sup>. To deeply understand the keyhole dynamic behavior in DP-VPTIG welding process, it is necessary to investigate the effect of the forces on the keyhole. As seen in Fig. 6, the arc pressure  $P_{a-z}$ , hydrostatic pressure  $P_h$  and surface tension  $P_s$  are the main forces that determine the behavior of keyhole. The arc pressure  $P_{a-z}$  is a downward force that tends to induce the depression of the weld pool surface, while the hydrostatic pressure  $P_h$  and the surface tension  $P_s$  are upward forces against  $P_{a-z}$ . To maintain the stable existence of the keyhole, the downward force  $P_{a-z}$  should be balanced with the upward forces  $P_s$  plus  $P_h$ . The equilibrium equation of the three forces can be given as:

$$P_{a-z} = P_h + P_s \quad (1)$$

$P_{a-z}$  can be represented by Eq.(2):

$$P_{a-z} = \frac{\mu I^2}{8\pi} \left( 1 + 2 \ln \frac{R_B}{R_E} \right) \quad (2)$$

where  $\mu$  is the permeability of the arc atmosphere,  $I$  is the welding current,  $R_E$  is the radius of the arc near the electrode, and  $R_B$  is the radius of the arc near the work-piece. From the equation,  $P_{a-z}$  is proportional to the square of the welding current.

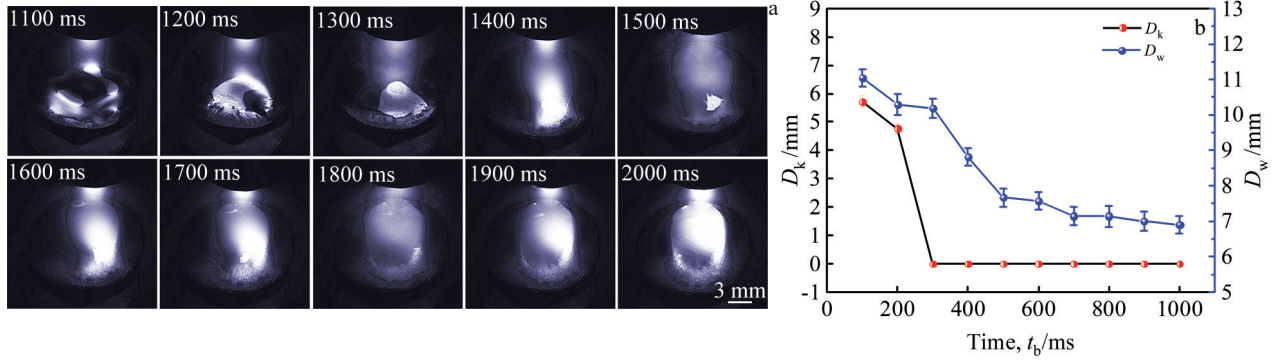


Fig.5 Keyhole appearance evolution process in low-pulsed base stage  $t_b$  (a); weld pool width  $D_w$  and keyhole size  $D_k$  (b)

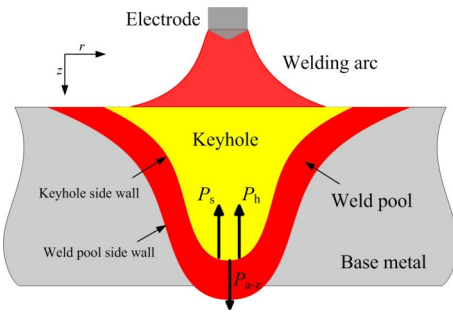


Fig.6 Force analysis at the bottom of keyhole

$P_h$  can be expressed as:

$$P_h = \rho g z \tag{3}$$

where  $\rho$  is the density of the liquid metal,  $g$  is the gravitational acceleration, and  $z$  is the depth to the entrance of the keyhole. It is obvious that  $P_h$  is proportional to the keyhole depth.

The surface tension  $P_s$  follows Young-Laplace equation expressed as

$$P_s = \frac{2\gamma}{R} \tag{4}$$

where  $R$  is the radius of curvature, and  $\gamma$  is the coefficient of surface tension.

During DP-VTIG welding process, in low-pulsed peak stage  $t_p$ , the welding current value is relatively high. The downward force  $P_{a-z}$  is higher than the upward forces  $P_s$  plus  $P_h$ , so that the downward force plays the dominant role in determining the keyhole dynamic in this stage. The keyhole forms as the weld pool surface moves downwards, and its depth keeps increasing with the duration of  $t_p$ . Meanwhile,  $P_s$  and  $P_h$  both increase with the increase of keyhole depth according to Eq.(3) and Eq.(4). As the sum of upward forces  $P_s+P_h$  reaches the value equal to  $P_{a-z}$ , Eq. (1) is then established. The keyhole in the weld pool reaches a quasi-stable state in  $t_p$ . When the current alters to low-pulsed base stage  $t_b$ ,  $P_{a-z}$  will decrease greatly caused by the dramatic reduction of the current value. Therefore, the upward forces  $P_s$  and  $P_h$  become the dominant role in determining the keyhole dynamic. Therefore, the bottom surface of keyhole moves upwards, accompanied by the decrease of weld pool surface depression. As keyhole depth decreases, the upward forces  $P_s$

and  $P_h$  both decrease. When the sum of upward forces  $P_s$  and  $P_h$  is equal to the downward force  $P_{a-z}$ , Eq.(1) is established again. Then, the keyhole behavior reaches another quasi-stable state in  $t_b$ .

With  $t_p$  providing the sufficient arc force to penetrate through the weld pool, and  $t_b$  significantly reducing the heat input, the stable keyhole mode welding of aluminium alloy is successfully achieved. The periodic variation in low-frequency pulsed current stimulates a periodic keyhole behavior of “opening” and “closing” inside the weld pool.

### 2.2 Effect of keyhole on weld penetration

According to the force analysis, the low-pulsed peak current  $I_{pp}$  plays a critical role in determining the formation of keyhole through affecting the maximum arc force during  $t_p$ . To investigate the effect of keyhole on weld penetration, trials were carried out with  $I_{pp}$  ranging from 210 A to 360 A. As observed in the above section, the weld pool and keyhole appearance at 1000 ms are sustained in a stable state in  $t_p$ . Here, the keyhole images were all captured at 1000 ms with different  $I_{pp}$ .

Fig.7 reveals the appearances of keyhole, the cross-section profile of the weld bead and corresponding characteristic sizes with increasing  $I_{pp}$ . As  $I_{pp}$  increases from 210 A to 360 A, the weld pool width  $D_w$  increases monotonously from 8 mm to 13.5 mm due to a higher heat input. Almost no keyhole forms when  $I_{pp}$  is less than 260 A. This is mainly because the downward arc force generated by this current level is insufficient to overcome the upward surface tension. Namely, a threshold current value, around 260 A in this condition, is needed for the formation of keyhole. As  $I_{pp}$  becomes higher, the depressed deformation of the weld pool surface is significantly increased, with the formation of a deep penetrated keyhole inside the weld pool. Meanwhile, the keyhole size  $D_k$  increases from 2.1 mm to 5.8 mm. The weld width  $W_{weld}$  is basically the same as the weld pool width  $D_w$ . The weld depth  $D_{weld}$  is 3.8 mm when  $I_{pp}$  is 260 A and is 7 mm when  $I_{pp}$  is 310 A. It means that there is a saltation in weld depth when the current increases from 260 A to 310 A, which is consistent with the keyhole size  $D_k$ . The ratio of  $D/W$  shows that the welding penetrating ability increases greatly when  $I_{pp}$  is higher than 260 A.

From the results, the weld penetration depth  $D_{weld}$  is

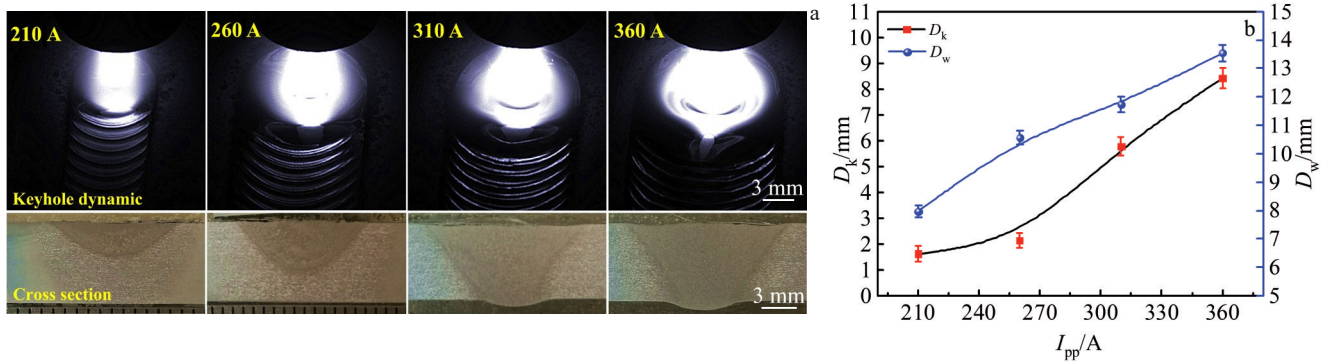


Fig.7 Effect of  $I_{pp}$  on keyhole and weld formation: (a) appearance of weld pool and cross-section; (b) weld pool width  $D_w$  and keyhole size  $D_k$  ( $I_{pp}$  =210, 260, 310, 360 A,  $I_{bp}$  =120 A,  $f_L$  =2 Hz, duty cycle=50%)

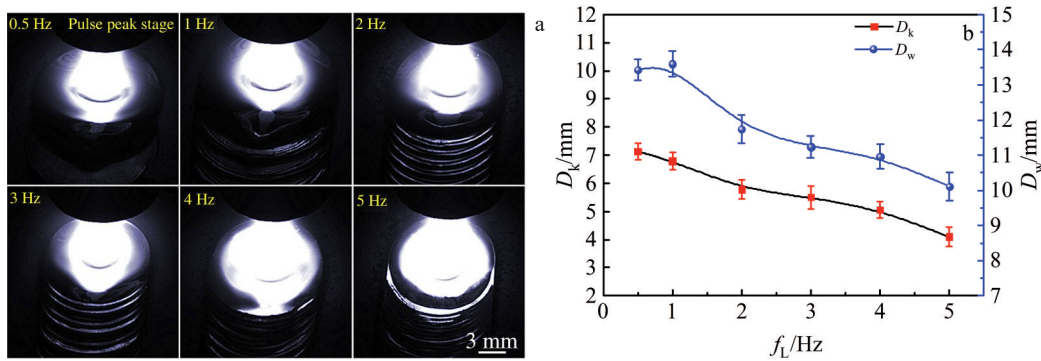


Fig.8 Effect of low-pulsed frequency on keyhole formation: (a) appearance of weld pool and keyhole; (b) weld pool width  $D_w$  and keyhole size  $D_k$  ( $I_{pp}$  =360 A,  $I_{bp}$  =120 A,  $f_L$  =0.5~5 Hz, duty cycle=50%)

simultaneously affected by the welding current  $I_{pp}$  and keyhole size  $D_k$ . To better understand the relationship among  $D_{weld}$ ,  $I_{pp}$  and  $D_k$ , regression analysis was performed, taking  $D_{weld}$  as the response of  $D_k$  and the square of  $I_{pp}$ . The regression equation can be expressed by:

$$D_{weld} = 1.6449 + 1.746 \times 10^{-5} I_{pp}^2 + 0.4463 D_k \quad (R^2 = 0.87) \quad (5)$$

From the results, the weld penetration depth is greatly affected by the formation of keyhole in addition to the welding current. The formation of keyhole inside the weld pool is beneficial to the increase of the weld penetration depth. As welding arc moves downwards along the keyhole, the solid base metal under the weld pool can be directly heated by the welding arc, rather than the heat conduction from the weld pool. The welding efficiency will be largely enhanced after the formation of keyhole in the weld pool.

### 2.3 Effect of low-pulsed frequency on keyhole formation

To understand the effect of low-pulsed frequency on keyhole formation, trials were undertaken with changing  $f_L$  from 0.5 Hz to 5 Hz. Fig.8 shows the appearance of weld pool and keyhole during  $t_p$ . It can be seen that under the condition of the same current value, the appearance of weld pool and keyhole differs largely at different  $f_L$ . As  $f_L$  increases, the weld pool width  $D_w$  presents a downward trend, decreasing from 13.4 mm at 0.5 Hz to 10.1 mm at 5 Hz. The keyhole size  $D_k$  exhibits a similar trend as  $D_w$  does. It decreases from 7.1 mm

at 0.5 Hz to 4.1 mm at 5 Hz. The keyhole size  $D_k$  shows an approximately linear changing trend with  $f_L$ , following the fitted Eq. (7). This is mainly because the pulse period decreases as the pulse frequency increases, leading to a decrease in residence time of pulse peak current in a complete pulse period.

$$D_k = 7.38 - 0.63 f_L \quad (6)$$

## 3 Conclusions

1) During DP-VPTIG keyhole mode welding, the keyhole forms in low-pulsed peak stage  $t_p$  due to the dominant role of downward arc force  $P_{a-z}$ . The keyhole is closed in low-pulsed base stage  $t_b$  as the upward forces surface tension  $P_s$  and hydrostatic pressure  $P_h$  become the dominant role. The periodic variation in low-frequency pulsed current stimulates a periodic keyhole behavior of “opening” and “closing” in the weld pool.

2) The threshold value of low-pulsed peak current  $I_{pp}$  for the formation of keyhole is about 260 A. The formation of keyhole is beneficial to the increase of the weld penetration depth as the arc moves downwards along the keyhole, thus directly heating the solid base metal under the weld pool.

3) The weld pool width  $D_w$  and keyhole size  $D_k$  both decrease with the increase of low-pulsed frequency  $f_L$ .

## References

- 1 Cong B Q, Ding J L, Williams S et al. *International Journal of Advanced Manufacturing Technology*[J], 2013, 76: 1593
- 2 Zhang P, Chen M H, Xie L S et al. *Rare Metal Materials and Engineering*[J], 2020, 49(3): 819
- 3 Li Q, Wang G Q, Dong M H et al. *Rare Metal Materials and Engineering*[J], 2021, 50(5): 1649
- 4 Wang Y P, Qi B J, Cong B Q et al. *Journal of Materials Processing Technology*[J], 2017, 249: 89
- 5 Wang L L, Wei J H, Wang Z M et al. *International Journal of Advanced Manufacturing Technology*[J], 2018, 95: 2421
- 6 Howse D S, Lucas W. *Science and Technology of Welding and Joining*[J], 2013, 5(3): 189
- 7 Jerzy N. *Welding International*[J], 2014, 28(1): 45
- 8 Jarvis B L, Ahmed N U. *Science and Technology of Welding and Joining*[J], 2000, 5(1): 1
- 9 Liu Z M, Chen S Y, Liu S et al. *International Journal of Heat and Mass Transfer*[J], 2018, 123: 54
- 10 Lathabai S, Jarvis B L, Barton K J. *Science and Technology of Welding and Joining*[J], 2008, 13(6): 573
- 11 Lathabai S, Jarvis B L, Barton K J. *Materials Science & Engineering A*[J], 2001, 299: 81
- 12 Lohse M, Fussel U, Schuster H. *Welding in the World*[J], 2013, 57: 735
- 13 Olivares E A G, Silva R H G, Dutra J C. *Welding International* [J], 2015, 20(3): 262
- 14 Feng Y Q, Luo Z, Liu Z M et al. *Materials & Design*[J], 2015, 85: 24
- 15 Liu Z M, Fang Y X, Qiu J Y et al. *Journal of Materials Processing Technology*[J], 2017, 250: 132
- 16 Cui S W, Shi Y H, Sun K. *Materials Science & Engineering A* [J], 2018, 709: 214
- 17 Fang Y X, Liu Z M, Cui S L et al. *Journal of Materials Processing Technology*[J], 2017, 250: 280
- 18 Cui S L, Liu Z M, Fang Y X et al. *Journal of Materials Processing Technology*[J], 2017, 243: 217
- 19 Wang Y P, Qi B J, Cong B Q et al. *Journal of Manufacturing Processes*[J], 2018, 34: 179
- 20 Yang M X, Li L, Qi B J et al. *Science and Technology of Welding and Joining*[J], 2017, 22(7): 580
- 21 Yang M X, Zheng H, Qi B J et al. *Journal of Materials Processing Technology*[J], 2017, 243: 9
- 22 Wang Y P, Cong B Q, Qi B J et al. *Journal of Materials Processing Technology*[J], 2019, 266: 255
- 23 Wang Y P, Qi B J, Cong B Q et al. *Rare Metal Materials and Engineering*[J], 2018, 47(11): 3522

## 2219 高强铝合金双频复合脉冲 VPTIG 焊接受激脉冲小孔行为

尹玉环<sup>1</sup>, 王义朋<sup>2</sup>, 高焯<sup>1</sup>, 钟豪<sup>3</sup>, 齐铂金<sup>3</sup>, 张铁民<sup>4</sup>, 从保强<sup>3</sup>

(1. 上海航天设备制造总厂, 上海 200245)

(2. 北京工业大学 材料与制造学部 轻合金材料与加工研究所, 北京 100124)

(3. 北京航空航天大学 机械工程及自动化学院, 北京 100191)

(4. 北京卫星制造厂, 北京 100086)

**摘要:** K-TIG (Keyhole TIG) 是 TIG 焊接工艺的一种变体, 通过在熔池内部形成小孔, 大幅提高焊缝熔深。然而, 由于铝合金热导率较高, K-TIG 通常被认为不适用于铝合金焊接。采用一种新型双频复合脉冲变极性 TIG (DP-VPTIG) 焊接工艺, 成功实现了 7 mm 厚 2219 高强铝合金的稳定全熔透小孔焊接。采用视觉传感技术研究了 DP-VPTIG 焊接小孔瞬态行为及其动态演变过程。结果表明, 熔池表面同时受到向上的电弧压力以及向下的表面张力和静水压力作用。DP-VPTIG 低频脉冲峰值阶段, 在电弧压力主导作用下熔池表面发生凹陷变形并在熔池内部形成深熔小孔; 低频脉冲基值阶段, 在表面张力和静水压力的主导作用下, 熔池表面上移, 小孔闭合。DP-VPTIG 焊接过程中低频脉冲的周期性变化激发了熔池内部小孔的周期性“打开”和“闭合”。小孔的形成使电弧沿熔池表面下移, 直接加热熔池下部的固态金属, 有利于焊缝熔深的提升, 且小孔尺寸随低频脉冲频率的增加而减小。

**关键词:** 小孔焊接; 双脉冲; 钨极氩弧焊; 铝合金

作者简介: 尹玉环, 女, 1981 年生, 博士, 研究员, 上海航天设备制造总厂, 上海 200245, E-mail: yinyuhuan149@163.com